International Journal of Solids and Structures 48 (2011) 2304–2309

Contents lists available at ScienceDirect

International Journal of Solids and Structures

journal homepage: www.elsevier.com/locate/ijsolstr

Cohesive modeling of crack nucleation in a cylindrical electrode under axisymmetric diffusion induced stresses

Tanmay K. Bhandakkar [1], Huajian Gao *

School of Engineering, Brown University, Providence, RI 02912, United States

ARTICLE INFO

Article history:
Received 2 June 2010
Received in revised form 18 March 2011
Available online 27 April 2011

Keywords:
Intercalation–deintercalation
Diffusion-induced stress
Lithium electrodes
Fracture
Flaw tolerance
Cohesive zone
Nanowire

ABSTRACT

We have recently modeled crack nucleation in a 2D strip electrode as localization of a periodic array of cohesive zones subject to diffusion induced stresses in an initially crack-free thin strip under galvanostatic solute insertion and extraction. Here we generalize this model to crack nucleation in a cylindrical electrode under axisymmetric diffusion induced stresses, focusing on the effect of the cylindrical geometry on the crack nucleation condition. Similar to our previous findings for the 2D strip geometry, the present analysis identifies a critical electrode size, typically in the nanometer range, to avoid crack nucleation.

1. Introduction

The technological needs to develop damage resistant lithium-ion battery electrodes with very large stresses and volume changes during Li intercalation–deintercalation cycles are calling for studies on crack nucleation under diffusion induced stresses. In the past, numerous models have been developed to describe the insertion/extraction of Li in an electrode as diffusion of interstitial atoms in a host material (García et al., 2005; Christensen and Newman, 2006a,b; Zhang et al., 2007, 2008; Cheng and Verbrugge, 2008, 2009; Deshpande et al., 2010a,b; Haftbaradaran et al., 2010, 2011; Yang, 2010), a subclass of problems more broadly referred to as the diffusion induced stresses (DIS) (Prussin, 1961; Li, 1978; Yang, 2005). In comparison, relatively few studies have explicitly considered crack nucleation under DIS. Huggins and Nix (2000) considered a bilayer plate with the top layer subjected to a swelling transformation strain and the bottom layer containing a crack. The Huggins–Nix model has been extended to the case of non-uniform distribution of DIS to predict relationships between charging rate, size and fracture toughness of an electrode particle for preventing growth of pre-existing cracks (Woodford et al., 2010; Zhao et al., 2010, 2011). In contrast, we have developed a cohesive model of crack nucleation in a strip electrode under galvanostatic charge and discharge (Bhandakkar and Gao, 2010). Compared to the Huggins–Nix model and its extensions (Huggins and Nix, 2000; Woodford et al., 2010; Zhao et al., 2010, 2011) which used Griffith's criterion to predict a critical condition for crack growth, the Bhandakkar–Gao model considers spontaneous localization of a periodic array of cohesive zones during dynamic evolution of DIS in an initially crack-free electrode.

Recent years have seen the development of various forms of cylindrical electrodes such as nanorods, nanopillars and nanowires, with improved performance and cycle life compared to planar and spherical electrode geometries (Taberna et al., 2006; Chan et al., 2008). The exact mechanism behind the superior mechanical response of cylindrical electrodes is unresolved and is being actively pursued (e.g. Huang et al., 2010). In the present paper, we extend the 2D Bhandakkar–Gao model to localization of an array of cohesive zones in a cylindrical electrode under axisymmetric diffusion induced stress as the maximum DIS exceeds the cohesive strength of the material (Fig. 1). Such localized deformation is thought to be initially reversible, and crack nucleation is assumed to occur when the maximum surface separation within the cohesive zone reaches a critical value.

2. Diffusion induced stress in a cylindrical electrode

Fig. 1 shows a cylindrical electrode with diameter $2r_c$ subject to insertion and extraction of an interstitial species such as Li. The electrode material is taken to be an isotropic linear elastic solid and the deformation is assumed quasi-static. Following an analogy

* Corresponding author. Tel.: +1 401 8632626, fax: +1 401 8639025.
E-mail address: Huajian_Gao@Brown.edu (H. Gao).
[1] Present address: Department of Mechanical Science and Engineering, University of Illinois at Urbana-Champaign, Urbana, IL 61801, USA.

0020-7683/$ - see front matter © 2011 Elsevier Ltd. All rights reserved.
doi:10.1016/j.ijsolstr.2011.04.005

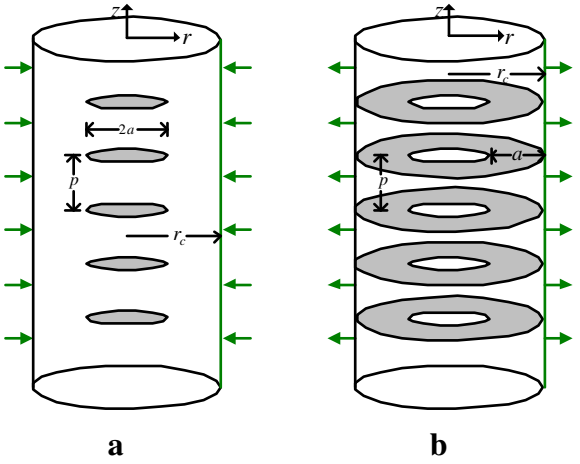

Fig. 1. Schematic illustration of crack nucleation in a cylindrical electrode of diameter $2r_c$ during galvanostatic (a) intercalation and (b) extraction, modeled as diffusion along the radial direction (r-axis). The axisymmetric crack nuclei are uniformly spaced with period p and modeled as localized cohesive zones obeying the triangular traction-separation law (Eq. (11)).

between DIS (Zhang et al., 2007, 2008; Cheng and Verbrugge, 2008, 2009; Deshpande et al., 2010a,b; Haftbaradaran et al., 2010, 2011; Yang, 2010) and thermal stresses, the transport of solute in the cylinder is modeled as a concentration driven diffusion process along the radial (r) direction of the electrode (Crank, 1980),

$$\frac{\partial c}{\partial t} = D\frac{1}{r}\frac{\partial}{\partial r}\left(r\frac{\partial c}{\partial r}\right), \tag{1}$$

where D is the diffusivity and c is the molar concentration of solute. The insertion of solute atoms into host causes a swelling transformation strain $\Omega c/3$, Ω being the partial molar volume of solute, which generates the following axial stress in the electrode (Timoshenko and Goodier, 1970),

$$\sigma_D(r,t) = \frac{E\Omega}{3(1-\nu)}\left[\frac{2}{r_c^2}\int_0^{r_c} r'c(r',t)dr' - c(r,t)\right], \tag{2}$$

where E is the Young's modulus and ν the Poisson ratio of the material.

Consider the variations of solute concentration and the corresponding DIS during charging and discharging. The initial solute concentration in the electrode is assumed to be zero. Under galvanostatic boundary conditions as shown in Fig. 1,

$$-D\frac{\partial c}{\partial r}\bigg|_{r_c} = -\frac{I}{F}; \quad -D\frac{\partial c}{\partial r}\bigg|_{0} = 0, \tag{3}$$

where I is the surface current density and F = 96486.7 C/mol is Faraday's constant, the solute concentration during insertion can be found as (Crank, 1980)

$$\frac{c(r,t)}{Ir_c/FD} = \frac{2Dt}{r_c^2} + \frac{r^2}{2r_c^2} - \frac{1}{4} - 2\sum_{n=1}^{\infty}\frac{J_0(\alpha_n r/r_c)}{\alpha_n^2 J_0(\alpha_n)}\exp\left\{-\frac{Dt\alpha_n^2}{r_c^2}\right\}, \tag{4}$$

and the associated DIS is

$$\sigma_D(r,t) = \frac{E\Omega}{3(1-\nu)}\frac{Ir_c}{FD}\left[\frac{1}{4} - \frac{r^2}{2r_c^2} + 2\sum_{n=1}^{\infty}\frac{J_0(\alpha_n r/r_c)}{\alpha_n^2 J_0(\alpha_n)}\exp\left\{-\frac{Dt\alpha_n^2}{r_c^2}\right\}\right], \tag{5}$$

where $J_0(r)$ is the Bessel function of the first kind and α_n are the roots of $J_1(\alpha)$. At the end of charging, the stress approaches a steady state while the solute concentration rises steadily with time. This situation persists until the saturation limit of material is reached. The steady state solution then acts as the initial condition for the extraction process,

$$c(r,0) = c_1 + \frac{Ir_c}{FD}\left[\frac{r^2}{2r_c^2} - \frac{1}{4}\right], \tag{6}$$

where

$$c_1 = \frac{2It_c}{Fr_c}, \tag{7}$$

t_c denoting the charging time. During extraction, the solute concentration evolves as

$$\frac{c(r,t) - c_1}{Ir_c/FD} = -\frac{2Dt}{r_c^2} - \frac{r^2}{2r_c^2} + \frac{1}{4} + 4\sum_{n=1}^{\infty}\frac{J_0(\alpha_n r/r_c)}{\alpha_n^2 J_0(\alpha_n)}\exp\left\{-\frac{Dt\alpha_n^2}{r_c^2}\right\}, \tag{8}$$

with the associated DIS

$$\sigma_D(r,t) = \frac{E\Omega}{3(1-\nu)}\frac{Ir_c}{FD}\left[\frac{r^2}{2r_c^2} - \frac{1}{4} - 4\sum_{n=1}^{\infty}\frac{J_0(\alpha_n r/r_c)}{\alpha_n^2 J_0(\alpha_n)}\exp\left\{-\frac{Dt\alpha_n^2}{r_c^2}\right\}\right]. \tag{9}$$

Fig. 2 plots the variations of solute concentration and the associated DIS during the first charging and discharging cycle. During insertion, the solute concentration continuously rises with time (Fig. 2a) while the stress approaches a steady state with tension near the center and compression near the free surface of the electrode (Fig. 2b). The peak tensile stress occurs at the centre when reaching the steady state, with magnitude equal to (Fig. 2b)

$$\sigma_{peak} = E\Omega Ir_c/12(1-\nu)FD. \tag{10}$$

During extraction, the surface current is reversed, and the solute concentration continuously decreases with time (Fig. 2c) while the stress approaches a steady state with compression near the center and tension at the surface of the electrode. The peak tensile stress occurs at the surface with the same magnitude as Eq. (10) when reaching the steady state (Fig. 2d).

Note that the above solutions to DIS neglect a number of nonlinear coupling effects and may be oversimplified in a number of ways. The reader is referred to Christensen and Newman (2006) for some detailed discussions. The current density I in the surface flux boundary condition of Eq. (3) couples the diffusion induced stress problem with electrochemical kinetics described by the Butler–Volmer reaction (Newman and Thomas, 2004; Zhang et al., 2008; Golmon et al., 2010). Heat generation in the electrode during charge and discharge also affects DIS. A fully coupled electrochemical–mechanical model with heat generation identified resistive heating as the most important heat source for electrode particles (Zhang et al., 2008). By introducing a coupling between internal stresses and activation energy for diffusion, Haftbaradaran et al. (2010) discovered a class of nonconventional solutions to DIS with a surface choking instability once the product between electrode dimension and charging rate exceeds a critical value. The nonlinear coupling between DIS and solute concentration in high capacity electrodes was also demonstrated through validation of continuum modeling with atomistic simulations of hydrogen diffusion in nickel, taking into account the coupling between DIS and the activation energy for diffusion, an upper bound to solute concentration based on stoichiometric limit and a concentration-dependent binding energy between the host and solute (Haftbaradaran et al., 2011). The effect of concentration-dependent binding energy between the host and solute on DIS was also analyzed by Yang (2010) for the thin plate geometry. First principle calculations have shown

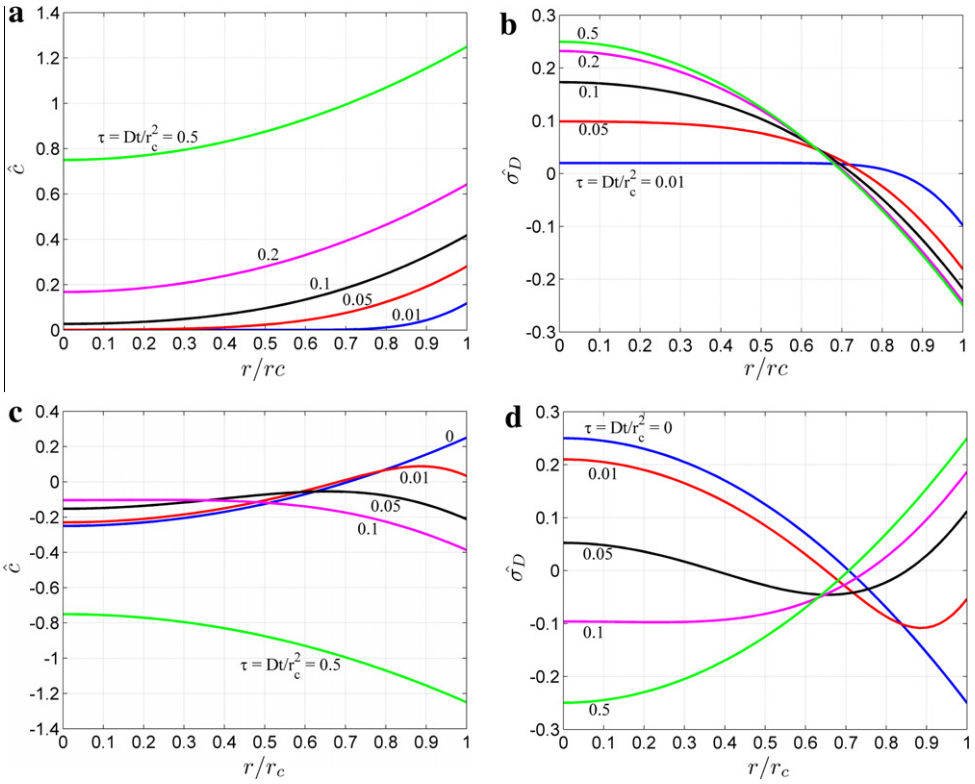

Fig. 2. Snapshot profiles of solute concentration and diffusion induced stress. (a) Concentration during insertion, (b) DIS during insertion, (c) concentration during extraction and (d) DIS during extraction. The concentration is normalized as $\hat{c} = cFD/(Ir_c)$ during insertion and $\hat{c} = (c - c_1)FD/(Ir_c)$ during extraction (Eqs. (4) and (8)), while DIS is normalized as $\hat{\sigma}_D = 3(1-\nu)FD\sigma_D/(E\Omega Ir_c)$ (Eqs. (5) and (9)).

that the Young's moduli of Li–Si phase decreases linearly with Li concentration relative to Si, even in the absence of amorphization (Shenoy et al., 2010). Stress measurement of a Si thin film on substrate has shown that the film undergoes plastic flow upon reaching its yield strength on the order of 1–1.75 GPa (Sethuraman et al., 2010). Xiao et al. (2011) studied crack spacing in Si thin films on Cu substrates and pointed out that the crack formation may be due to localization of plastic strain in Si. These effects will tend to smooth out the concentration and DIS profiles in the electrode, making our predictions based on the uncoupled formulation conservative in nature.

We can apply Eq. (10) to the recent charging-discharging experiments on silicon nanowire electrodes (Chan et al., 2008) and get an idea of the magnitude of diffusion induced stresses in high capacity electrodes. Silicon nanowire electrodes with an average diameter of 89 nm are found to be charged to near the theoretical capacity of 4227 mAh g^{-1} at a charge and discharge rate of 20 h per half cycle (Chan et al., 2008), corresponding to a surface current density of $I = 0.011$ A/m^2. For such electrodes the peak tensile stress during insertion and extraction is estimated to be 0.16 GPa. For a faster charge and discharge rates of 5 h per half cycle charged to a capacity of 3500 mAh g^{-1}, the surface current density is $I = 0.036$ A/m^2, corresponding to a peak stress of 0.53 GPa during Li insertion and extraction. The material parameters for the estimation can be found in our previous work[2] (Bhandakkar and Gao, 2010). In the following, we consider crack nucleation under these large diffusion induced stresses in the electrode which is assumed to be initially free of cracks.

[2] Numerator in Eq. (12) (Bhandakkar and Gao, 2010) should read as 3×0.59 instead of 4.

3. Cohesive model of crack nucleation in a cylindrical electrode

Consider crack nucleation as localization of a periodic array of cohesive zones in an initially crack-free electrode, as shown in Fig. 1. The cohesive zones are uniformly spaced at a period p near the center of the electrode during solute insertion and at the edge of the electrode during solute extraction. We adopt the triangular traction–separation ($\sigma - \delta$) law (Camacho and Ortiz, 1996),

$$\sigma = \begin{cases} \sigma_c(1 - \delta/\delta_c), & \delta \leqslant \delta_c, \\ 0, & \delta > \delta_c, \end{cases} \tag{11}$$

where σ_c is the cohesive strength of the electrode material and δ_c is the maximum range of cohesive interaction. The fracture energy of the material, $\Gamma = \sigma_c\delta_c/2$, is assumed to be a material constant typically on the order of surface energy in the absence of significant plastic deformation.

The emergent cohesive zones are modelled as continuous distributions of prismatic dislocations loops (Bilby and Eshelby, 1968). During solute insertion, the cohesive zones would develop at the centre of the electrode as soon as the stress exceeds the cohesive strength. Within the cohesive zone, the traction and the surface separation obey Eq. (11), i.e.

$$\sigma_D(r,t) + \int_0^a P(r,R)B(R,t)dR = \sigma_c\left(1 - \frac{\sigma_c}{2\Gamma}\int_r^a B(R,t)dR\right), \quad 0 \leqslant R \leqslant a, \tag{12}$$

where the first term $\sigma_D(r,t)$ is the diffusion induced stress and the second term is the stress associated with localized deformation within the cohesive zones modeled as continuous distributions of prismatic dislocation loops of radius R with density $B(R,t)$.

The kernel function $P(r, R)$ in Eq. (12) corresponds to the axial stress at location $(r, 0)$ induced by an infinite array of coaxial prismatic dislocation loops of unit Burgers vector in the z-direction and radius R, located at positions $z = np$; $n = -\infty, \ldots, \infty$ along the axis. In practice, since the stress field associated with a prismatic loop in a cylinder decays cubically (Kroupa, 1960) with distance along the axis of the cylinder, we determine $P(r, R)$ from 5 prismatic loops with spacing p along the cylindrical axis. Similar approximation has been adopted previously in studying interaction among periodic array of cracks in a layer (Bai et al., 2000). The expression for $P(r, R)$ is given in Supplementary material 1. Similar to the Dugdale model (Dugdale, 1960), the cohesive zone size is determined based on the condition that there exists no singularity at the tip of the cohesive zone,

$$\lim_{r\to a} B(r,t)\sqrt{a-r} = 0, \tag{13}$$

and crack nucleation is assumed to occur when the maximum surface separation reaches $\delta_c = 2\Gamma/\sigma_c$, i.e.

$$\int_0^a B(R,t)dR = 2\Gamma/\sigma_c. \tag{14}$$

Finally, the spacing p between the cohesive zones is determined by the condition that the axial stress everywhere in the electrode must not exceed the cohesive strength.

During solute extraction, the tensile stress region is shifted to the surface of the electrode while the centre of the electrode is under compression. Therefore, the emergent cohesive zones are placed periodically along the edge of the electrode with governing equation

$$\sigma_D(r,t) + \int_{r_c-a}^{r_c} P(r,R)B(R,t)d\eta = \sigma_c\left(1 + \frac{\sigma_c}{2\Gamma}\int_{r_c-a}^{r} B(R,t)dR\right), \quad r_c - a \leqslant R \leqslant r_c. \tag{15}$$

In this case, the size of the cohesive zones is determined based on

$$\lim_{r\to r_c-a} B(r,t)\sqrt{r-r_c+a} = 0, \tag{16}$$

and the corresponding crack nucleation condition is

$$\int_{r_c}^{r_c-a} B(R,t)dR = 2\Gamma/\sigma_c. \tag{17}$$

Normalizing all stress variables by σ_c and all length variables by r_c in Eqs. (5), (9) and (12)–(17), we can identify a characteristic length scale as

$$\ell_{ft} = \left\{\frac{\Gamma(1-\nu)F^2D^2}{E(1+\nu)\Omega^2I^2}\right\}^{1/3}. \tag{18}$$

4. Localization spacing p

Following our previous study of crack nucleation in a strip electrode (Bhandakkar and Gao, 2010), we assume that the localization process would naturally select the cohesive zone spacing such that the maximum axial stress in the region between two adjacent cohesive zones is exactly equal to the cohesive strength σ_c.

For the formation of centre cohesive zones during solute insertion (Fig. 1a), the maximum axial stress in the region between two adjacent cohesive zones occurs along the axis of the cylinder right in the middle of the two localization zones. Hence, the cohesive zone spacing p is determined by solving

$$\sigma_z(0,p/2) = \sigma_D(0,t) + \int_0^a H(0,p/2,R)B(R,t)dR = \sigma_c, \tag{19}$$

together with Eqs. (12)–(14). The kernel function $H(r, z, R)$ corresponds to the axial stress at (r, z) induced by an array of five coaxial circular prismatic dislocation loops of unit Burgers vector in the z-direction and radius R, located at $z = np$; $n = -2, \ldots, 2$ along the axis. The expression for kernel function $H(r, z, R)$ is given in Supplementary material 1. For a given cohesive strength σ_c, we solve Eqs. (12)–(14), followed by checking Eq. (19) and employing the method of bisection to determine p.

For the formation of edge cohesive zones during solute extraction (Fig. 1b), the maximum axial stress in the region between two adjacent cohesive zones occurs along the free surface at the midpoint between the two localization zones. The cohesive zone spacing p is then determined by solving

$$\sigma_z(r_c,p/2) = \sigma_D(r_c,t) + \int_{r_c-a}^{r_c} H(r_c,p/2,R)B(R,t)dR = \sigma_c, \tag{20}$$

together with Eqs. (15)–(17). We will focus on crack nucleation under a steady state phase after the initial transient has passed but before the maximum stoichiometric solute concentration of the host material is reached. Fig. 3a and b plot the cohesive zone spacing as a function of the cohesive strength during solute insertion and extraction, respectively. Once the localization spacing p is determined, the critical conditions for crack nucleation are obtained from Eqs. (12)–(14) for center cracks during solute insertion and from Eqs. (15)–(17) for edge cracks during solute extraction by a numerical scheme detailed in Supplementary material 2.

In contrast to the periodic array of localization zones of Fig. 3, nucleation of isolated localization zone is possible in case the peak DIS is smaller than the cohesive strength of electrode material. Such a solution is *metastable* and may occur at locations with pre-existing defects/weaknesses. The governing equations and numerical algorithm for such metastable, isolated localizations

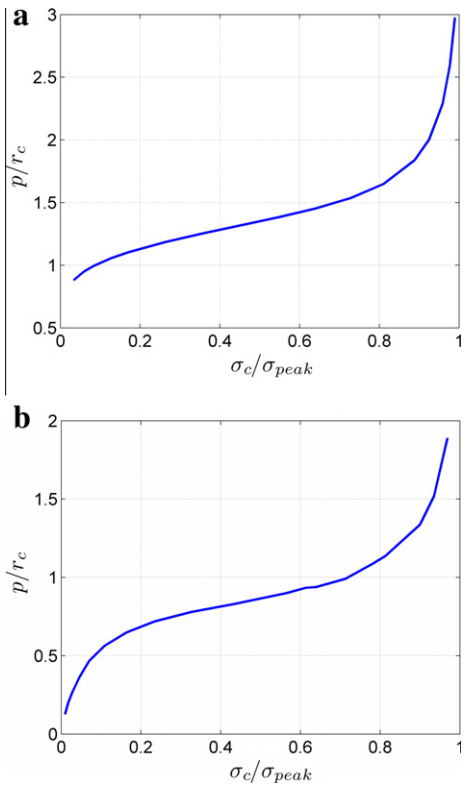

Fig. 3. Localization spacing p as a function of the normalized cohesive strength for the formation of (a) centre cohesive zones during solute insertion and (b) edge cohesive zones during solute extraction. In both (a) and (b), the cohesive strength σ_c is normalized by the peak DIS $\sigma_{peak} = E\Omega I r_c/[12(1-\nu)FD]$.

are similar to those for spontaneous localizations, except the Green's function kernel is replaced with $S(r, R)$ which corresponds to the axial stress at location $(r, 0)$ induced by a single coaxial circular prismatic dislocation loop of a unit burgers vector in the z-direction and radius R with center located at $z = 0$. The expression for $S(r, R)$ is given in Supplementary material 1. Fig. 4 indicates that the critical radius and cohesive zone size undergo smooth transition between multiple localization to isolated localization regimes.

5. Comparison of critical conditions for crack nucleation between cylinder and strip

The normalized radius of the electrode and the cohesive strength normalized by the corresponding peak stress in the electrode are related by the blue solid lines in Fig. 4a and b. The critical size of the cohesive zone at crack nucleation as a function of the normalized cohesive strength is shown in green dashed lines.

A comparison of the present results with our previous work on crack nucleation in a strip electrode (Bhandakkar and Gao, 2010) reveals that the cylindrical geometry does not alter the relationships between cohesive strength, characteristic electrode size and cohesive zone size qualitatively. There exists a critical electrode dimension below which crack nucleation becomes impossible *irrespective of the cohesive strength of the material*. This critical dimension is found to be $r_{cr}^{I} = 7.3\ell_{ft}$ during solute insertion (which is identical to the corresponding critical dimension in the case of a strip) and $r_{cr}^{E} = 8.2\ell_{ft}$ during solute extraction (the corresponding critical dimension in the case of a strip is $6.5\ell_{ft}$); see Fig. 4a and b. This analysis suggests that crack nucleation is more likely to occur at the center of electrode during solute insertion, as opposed to nucleation at the edge of electrode during solute extraction. This deviates from our previous analysis (Bhandakkar and Gao, 2010) where crack nucleation at the edge of the electrode is found to be more likely. In reality, stress concentration induced by surface roughness may aid crack nucleation at the surface of electrodes during solute extraction. A critical dimension for flaw tolerant cylindrical electrodes is thus identified as

$$2r_{cr} = 14.6\ell_{ft} = 14.6\left\{\frac{\Gamma(1-\nu)(FD)^2}{E(1+\nu)(\Omega I)^2}\right\}^{1/3}. \tag{21}$$

The significance of this equation is that it predicts an initially crack-free electrode would remain crack free below the critical dimension. Once the electrode diameter exceeds this critical dimension, nucleation of center circular cracks during solute insertion would become possible. The plots in Fig. 4a and b are based on cohesive strength normalized by the peak tensile stresses during solute insertion and extraction. In order to decouple the effect of electrode size and cohesive strength, we introduce a size-independent reference stress $\sigma_{ref} = E\Omega I\ell_{ft}/12(1-\nu)FD$ and replot the results of Fig. 4a and b in Fig. 4c and d based on a new normalization of the cohesive strength with respect to σ_{ref}. The critical dimension for crack nucleation increases almost linearly with cohesive strength for very large as well as very small values of σ_c/σ_{ref}. The peculiar behavior at small values of σ_c/σ_{ref} is owing to the large cohesive interaction range δ_c under the constraint of constant fracture energy $\Gamma = \sigma_c\delta_c/2$.

Following our previous study (Bhandakkar and Gao, 2010), we can estimate the critical dimension and current density for flaw tolerant electrodes based on Eq. (21). The critical dimension for flaw tolerant Si electrodes charged to near theoretical capacity at

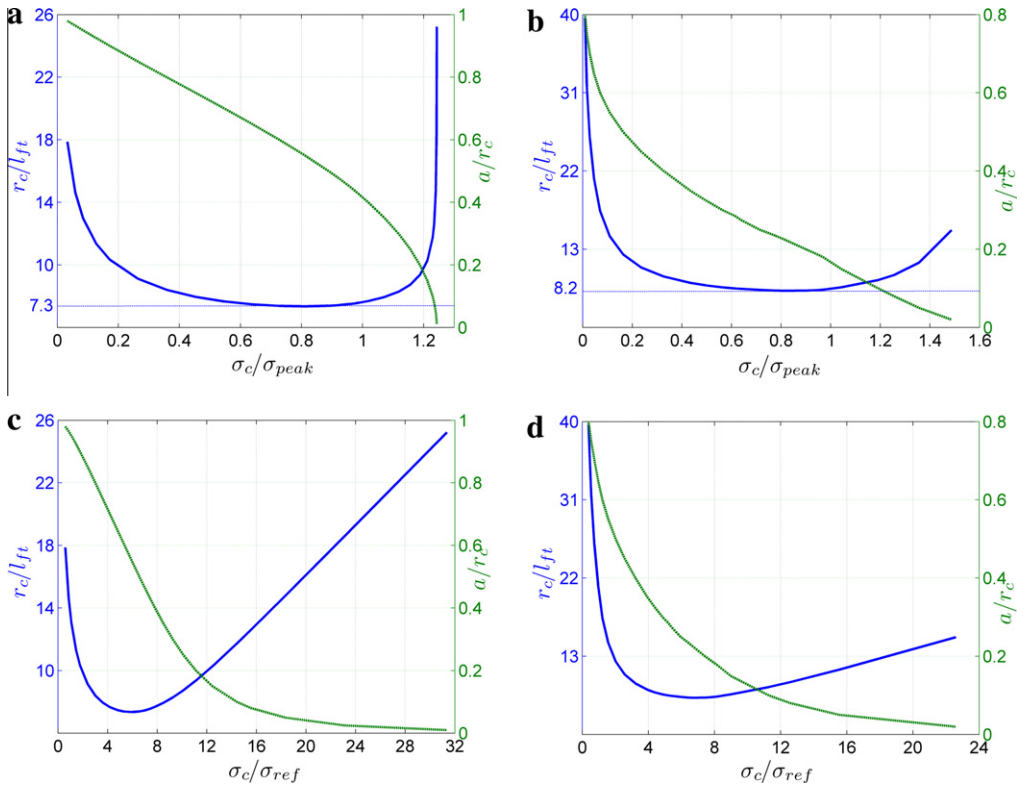

Fig. 4. The critical conditions for crack nucleation expressed as relationships between the normalized radius of electrode, the normalized cohesive strength and the normalized critical size of cohesive zone at nucleation. The blue lines plot the critical dimension of electrode while the dashed green lines plot the critical size of cohesive zone at crack nucleation as functions of the normalized cohesive strength. (a) and (c) plot the critical conditions for nucleation of center cohesive zones of radius a under solute insertion while (b) and (d) plot those of edge annular cohesive zones of size a under solute extraction. In (a), (b), the cohesive strength is normalized by the peak DIS $\sigma_{peak} = E\Omega I r_c/[12(1-\nu)FD]$. In (c) and (d), the cohesive strength is normalized by the size-independent reference stress $\sigma_{ref} = E\Omega I\ell_{ft}/[12(1-\nu)FD]$ where ℓ_{ft} is the characteristic length scale defined in Eq. (18). (For interpretation of the references to colour in this figure legend, the reader is referred to the web version of this article.)

a charge-discharge rate of 20 h per half cycle is estimated to be 467 nm, which falls in the experimental range of Chan et al. (2008). For nanowire of 89 nm in diameter adopted in experiments (Chan et al., 2008), we estimate that crack nucleation might occur in the Si nanowire at the charging-discharging rate of 1.6 h per half-cycle. Indeed, significant capacity loss is reported, as the charging/discharging rate changes to below 10 h per half cycle (Fig. 2c, Chan et al., 2008). Although the reasons for such capacity loss is not completely clear, the observation would be more or less consistent with our analysis if crack formation during charging is assumed to be a prime cause. The broad agreement between experiment and our analysis points to the fact that crack nucleation can indeed be suppressed in nanostructured electrodes and design of fracture resistant electrodes can greatly improve the cycling performance of Li batteries.

6. Summary and discussions

In this paper, we have extended our previous model (Bhandakkar and Gao, 2010) of crack nucleation in a strip electrode as localization of an array of cohesive zones under galvanostatic diffusion induced stresses to the corresponding three dimensional problem of a cylindrical electrode. It is shown that the cylindrical geometry does not appreciably change the results reported in Bhandakkar and Gao (2010). The present analysis reiterates the importance of nanoscale electrodes in preventing crack formation under large diffusion induced stresses. The most important result of our analysis is the existence of a critical electrode diameter

$$d_{ft} = 14.6\left\{\frac{\Gamma(1-\nu)F^2D^2}{E(1+\nu)\Omega^2 I^2}\right\}^{1/3}, \tag{22}$$

below which crack nucleation becomes impossible *irrespective of the cohesive strength of material,* and contributes towards the understanding of the success of nanowire geometries. Our analysis also highlights an inverse relationship between critical charging current and electrode dimension, whereby faster charging leads to higher stresses and more chances of crack nucleation. Similar to Bhandakkar and Gao (2010), we identify that a potential design criterion for flaw tolerant electrode is

$$I^{2/3}d \leqslant \text{crit}, \tag{23}$$

where I is the operating current and d the dimension of electrode. Once the critical value of $I^{2/3}d$ for "fail-safe" design of electrode is determined through careful set of experiments, Eq. (23) can be used to design the actual electrode dimension and current density.

Acknowledgement

Financial support from the National Science Foundation through Grant CMMI-0758535 is gratefully acknowledged.

Appendix A. Supplementary data

Supplementary data associated with this article can be found, in the online version, at doi:10.1016/j.ijsolstr.2011.04.005.

References

Bai, T., Pollard, D.D., Gao, H., 2000. Explanation for fracture spacing in layered materials. Nature 403, 753–756.

Bhandakkar, T.K., Gao, H., 2010. Cohesive modeling of crack nucleation under diffusion induced stresses in a thin strip: implications on the critical size for flaw tolerant battery electrodes. International Journal of Solids and Structures 47, 1424–1434.

Bilby, B.A., Eshelby, J.D., 1968. Dislocations and the theory of fracture. In: Liebowitz, H. (Ed.), Fracture, An Advanced Treatise. Microscopic and Macroscopic Fundamentals, vol. 1. Academic Press, New York and London, pp. 99–182.

Camacho, G.T., Ortiz, M., 1996. Computational modeling of impact damage in brittle materials. International Journal of Solids and Structures 33, 2899–2938.

Chan, C.K., Peng, H., Liu, G., McIlwrath, K., Zhang, X.F., Huggins, R.A., Cui, Y., 2008. High-performance lithium battery anodes using silicon nanowires. Nature Nanotechnology 3, 31–35.

Cheng, Y.-T., Verbrugge, M.W., 2008. The influence of surface mechanics on diffusion induced stresses within spherical nanoparticles. Journal of Applied Physics 104, 083521-1–083521-6.

Cheng, Y.-T., Verbrugge, M.W., 2009. Evolution of stress within a spherical insertion electrode particle under potentiostatic and galvanostatic operation. Journal of Power Sources 190, 453–460.

Christensen, J., Newman, J., 2006a. A mathematical model of stress generation and fracture in lithium manganese oxide. Journal of the Electrochemical Society 153, A1019–A1030.

Christensen, J., Newman, J., 2006b. Stress generation and fracture in lithium insertion materials. Journal of Solid State Electrochemistry 10, 293–319.

Crank, J., 1980. The Mathematics of Diffusion. Oxford University Press.

Deshpande, R., Cheng, Y.-T., Verbrugge, M.W., 2010a. Modeling diffusion-induced stress in nanowire electrode structures. Journal of Power Sources 195, 5081–5088.

Deshpande, R., Qi, Y., Cheng, Y.-T., 2010b. Effects of concentration-dependent elastic modulus on diffusion-induced stresses for battery applications. Journal of the Electrochemical Society 157, A967–A971.

Dugdale, D.S., 1960. Yielding of steel sheets containing slits. Journal of the Mechanics and Physics of Solids 8, 100–104.

García, R.E., Chiang, Y.-M., Carter, W.C., Limthongkul, P., Bishop, C.M., 2005. Microstructural modeling and design of rechargeable lithium-ion batteries. Journal of the Electrochemical Society 152, A255–A263.

Golmon, S., Maute, K., Lee, S.-H., Dunn, M.L., 2010. Stress generation in silicon particles during lithium insertion. Applied Physics Letters 97, 033111-1–033111-3.

Haftbaradaran, H., Gao, H., Curtin, W.A., 2010. A surface locking instability for atomic intercalation into a solid electrode. Applied Physics Letters 96, 091909-1–091909-3.

Haftbaradaran, H., Song, J., Curtin, W.A., Gao, H., 2011. Continuum and atomistic models of strongly coupled diffusion, stress, and solute concentration. Journal of Power Sources 196, 361–370.

Huang, J.Y., Zhong, L., Chong, M.W., Sullivan, J.P., Xu, W., Zhang, L.Q., Mao, S.X., Hudak, N.S., Xiao, H.L., Subramanian, A., Fan, H., Qi, L., Kushima, A., Li, J., 2010. In situ observation of the electrochemical lithiation of a single SnO_2 nanowire electrode. Science 330, 1515–1520.

Huggins, R.A., Nix, W.D., 2000. Decrepitation model for capacity loss during cycling of alloys in rechargeable electrochemical system. Ionics 6, 57–63.

Kroupa, F., 1960. Circular edge dislocation loop. Czechoslovak Journal of Physics 10B, 284–293.

Li, J.C.M., 1978. Physical chemistry of some microstructural phenomena. Metallurgical Transactions A 9, 1353–1380.

Newman, J., Thomas, K.E., 2004. Electrochemical Systems, third ed. Wiley, New York.

Prussin, S., 1961. Generation and distribution of dislocations by solute diffusion. Journal of Applied Physics 32, 1876–1881.

Sethuraman, V.A., Chon, M.J., Shimak, M., Srinivasan, V., Guduru, P.R., 2010. In situ measurements of stress evolution in silicon thin films during electrochemical lithiation and delithiation. Journal of Power Sources 195, 5062–5066.

Shenoy, V.B., Johari, P., Qi, Y., 2010. Elastic softening of amorphous and crystalline Li–Si Phases with increasing Li concentration: a first-principles study. Journal of Power Sources 195, 6825–6830.

Taberna, P.L., Mitra, S., Poizot, P.S., Simon, P., Tarascon, J.-M., 2006. High rate capabilities Fe_3 O_4-based Cu nano-architectured electrodes for lithium-ion battery applications. Nature Materials 5, 567–573.

Timoshenko, S.P., Goodier, J.N., 1970. Theory of Elasticity. McGraw-Hill Book Company.

Woodford, W.H., Chiang, Y.-M., Carter, W.C., 2010. "Electrochemical shock" of intercalation electrodes: A fracture mechanics analysis. Journal of the Electrochemical Society 157, A1052–A1059.

Xiao, X., Liu, P., Verbrugge, M.W., Haftbaradaran, H., Gao, H., 2011. Improved cycling stability of silicon thin film electrodes through patterning for high energy density lithium batteries. Journal of Power Sources 196, 1409–1416.

Yang, F., 2005. Interaction between diffusion and chemical stresses. Materials Science and Engineering A 409, 153–159.

Yang, F., 2010. Effect of local solid reaction on diffusion-induced stress. Journal of Applied Physics 107, 103516-1–103516-7.

Zhang, X., Shyy, W., Sastry, A.M., 2007. Numerical simulation of intercalation-induced stress in Li-ion battery electrode particles. Journal of the Electrochemical Society 154, A910–A916.

Zhang, X.C., Sastry, A.M., Shyy, W., 2008. Intercalation-induced stress and heat generation within single lithium-ion battery cathode particles. Journal of the Electrochemical Society 155, A542–A552.

Zhao, K., Pharr, M., Vlassak, J.J., Suo, Z., 2010. Fracture of electrodes in lithium-ion batteries caused by fast charging. Journal of Applied Physics 108, 073517-1–073517-6.

Zhao, K., Pharr, M., Vlassak, J.J., Suo, Z., 2011. Inelastic hosts as electrodes for high-capacity lithium-ion batteries. Journal of Applied Physics 109, 016110-1–016110-3.